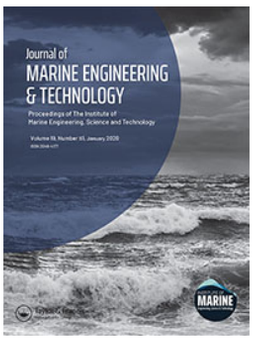

Taylor & Francis
Taylor & Francis Group

Journal of Marine Engineering & Technology

ISSN: 2046-4177 (Print) 2056-8487 (Online) Journal homepage: https://www.tandfonline.com/loi/tmar20

Robustness analysis of dual actuator EGR controllers in marine two-stroke diesel engines

Lars Eriksson & Xavier Llamas

To cite this article: Lars Eriksson & Xavier Llamas (2020) Robustness analysis of dual actuator EGR controllers in marine two-stroke diesel engines, Journal of Marine Engineering & Technology, 19:sup1, 17-30, DOI: 10.1080/20464177.2020.1712065

To link to this article: https://doi.org/10.1080/20464177.2020.1712065

Published online: 30 Jan 2020.

JOURNAL OF MARINE ENGINEERING & TECHNOLOGY
2020, VOL. 19, NO. S1, 17–30
https://doi.org/10.1080/20464177.2020.1712065

Taylor & Francis
Taylor & Francis Group

Robustness analysis of dual actuator EGR controllers in marine two-stroke diesel engines

Lars Eriksson and Xavier Llamas

Dept. of Electrical Engineering, Vehicular Systems, Linköping, Sweden

ABSTRACT

Exhaust Gas Recirculation (EGR) was recently introduced in large marine two-stroke diesel engines to reduce NO_x-emissions. Controlling EGR flow during accelerations, while keeping good acceleration performance is challenging, due to delays in the scavenge receiver oxygen measurement and upper limits on fuel for avoiding black smoke. Previous oxygen feedback controllers struggled during accelerations, but a new EGR-controller based on adaptive feedforward (AFF) has been successful. Nevertheless, further analysis and tests are required before deploying the controller to more EGR ships. A simulation platform is a great asset to test controllers before expensive real-world experiments are conducted. A new EGR flow controller is proposed and tested in a complete ship simulation model. Several acceleration scenarios show that the low load area is most challenging. Controller robustness is analysed in this area, showing that pressure sensor bias in the EGR flow estimator is the most critical factor, which could lead to black smoke formation. This can be prevented with sensor calibration or by using a differential pressure sensor. Errors in the parameters of the flow estimators are not as important. This is a useful result because the right parameters of the flow estimators might be difficult to obtain, on a new engine.

ARTICLE HISTORY
Received 8 May 2019
Accepted 16 December 2019

KEYWORDS
Split-range control; exhaust gas recirculation; marine pollution; engine control

1. Introduction

Developing a clean and efficient transportation sector is one of the most important goals for the society. Road transport started to define more strict emission limits of CO_2 and other pollutants several decades ago. While marine freight began to be regulated later, in the past years, significant steps have been taken to reduce its environmental impact. The latest is the stricter Tier III emission limit, which enforces a substantial NO_x reduction for vessels built after January 2016 in certain coastal NO_x Emission Control Areas (NECAs), see International Maritime Organization (2013).

One method to reduce the thermal NO_x formed during the combustion is Exhaust Gas Recirculation (EGR). By recirculating burned gases back into the cylinders, the heat capacity of the air is increased which results in lower cylinder peak temperatures and thus less NO_x formation, see Heywood (1988) for mechanisms and the basic principles. The application of EGR requires proper gas flow control to adjust and achieve the right amounts of air and exhaust flows at different loads and speeds. EGR flow control during steady state is not a significant challenge for these large engines. However, the difficulties arise when a specific EGR rate has to be maintained when the vessel is manoeuvering in a NECA. In addition, the reduced availability of oxygen during EGR operation limits the amount of fuel that can be burned without visible black smoke formation. This issue together with the industry trend to downsize the engines for fuel economy can reduce the vessel maneuverability. Moreover, the oxygen measurement contains inherent delays due to a required gas extraction process, which made the original PI feedback to perform poorly in these situations. Hence, better EGR controllers that more appropriately handle these acceleration scenarios are crucial for the emission reduction and introduction of EGR on marine diesel engines.

1.1. State of the art in marine diesel engine EGR control

The subsections below summarise results on Marine Engine Control. The majority of the marine diesel engine control research has been on the speed governor, i.e. engine RPM (and ship speed). EGR Control is a relatively new subject for two-stroke marine engines, it has evolved from four-stroke application but there are some key differences.

CONTACT Lars Eriksson lars.eriksson@liu.se

1.1.1. Engine processes

Internal combustion engines have made a profound impact on today's society and the subject is covered in several text books. The classic book Heywood (1988) gives a thorough treatment of the fundamental principles of internal combustion engines, including thermodynamics, combustion physics, fluid flow, heat transfer, emissions and much more. It has become the standard reference for engine processes. More recent texts with focus on engine modelling and control are Guzzella and Onder (2010) and Eriksson and Nielsen (2014). While these are focused on four-stroke automotive engines, many of the modelling and control concepts apply to two-stroke engines as well, since they are governed by the same physics.

Large two-strokes without EGR. The large two-stroke crosshead diesel engine has received less attention in the literature than the automotive four-stroke. The topic of governor (engine speed controller) design has attracted the most efforts around dynamic modelling of the large engines. A number of texts show the foundation: Woodward and Latorre (1985) discusses methods of modelling diesel engines for simulation of propulsion transients; Blanke and Andersen (1984) showed that the turbocharger inertia has a significant impact on the engine speed dynamics; the term mean value engine model (MVEM) was coined for two-stroke diesel engine in Hendricks (1986). Winterbone and Jai-In (1991) discusses how the introduction of electronic governors allowed for more advanced controller designs. An example was a multi-variable control system of diesel engine with VGT that improves transient fuel economy and smoke formation. Banning et al. (1997) presents how the combination of H_∞ control and non-linear techniques can be used for fuel efficiency optimisation. The increasingly strict emission constraints led Stefanopoulou and Smith (2000) to further investigate the use of VGT as an extra degree-of-freedom to mitigate the trade-off between optimising the engine for steady state and avoiding emissions during transients. Coordination of injected fuel and VGT area was proposed for control of the air/fuel-ratio. A multiple-input multiple-output controller is developed but not verified experimentally. Further treatment of governor design was given by Xiros (2002) that investigated the use of PID and linear-state-feedback methods for disturbance rejection and robustness. The design was based on a state-space model from physical, thermodynamic engine description and mapping using neural nets.

The necessity of filling-and-emptying dynamics in MVEMs of a marine two-stroke is investigated in Theotokatos (2010). It shows that a model with simplified dynamics (quasi-steady) can represent the engine speed response but only after increasing the turbocharger inertia parameter to indirectly include the dynamics of the scavenge and exhaust receivers. Models with filling-and-emptying dynamics were considered more appropriate for prediction of engine dynamics and for more advanced control system design studies. The quasi-steady model was used by Xiros and Theotokatos (2011) to map torque-response with neural nets, create a neural state-space model and suggest a supervisory speed control structure. The full model from Theotokatos (2010) was used by Guan et al. (2014) for investigation of engine performance and auxiliary blowers at low load. Guan et al. (2015) extended the model by replacing the cylinder block with a zero-dimensional model and used it for investigation of turbocharger cut-out and auxiliary blower activation in low load conditions. Theotokatos and Tzelepis (2015) used the full model from Theotokatos (2010) to map the performance and emission parameters of a ship and showed how the result could be used for minimising fuel consumption of a typical ship.

Four-stroke engines and EGR. Modelling and control of EGR in automotive four-stroke engines is a related area of research. In this area the interactions between the EGR valve, VGT and the nonlinearity of the system makes for an interesting control problem with a wide variety of proposed solutions (Nieuwstadt et al. 2000; Jankovic et al. 2000; Ammann et al. 2003; Wahlström et al. 2010; Wahlström and Eriksson 2011a, 2011b, 2013). Slow sensor dynamics have led to research in observers, feedforward and other methods of compensation for engines with and without EGR (Jankovic and Kolmanovsky 2009; Yildiz et al. 2010; Tschanz et al. 2013). Observer designs have also been proposed for cost reduction or to estimate engine variables that are difficult to measure (Zhao and Wang 2013; Poloni et al. 2014; Zhao and Wang 2015).

Large two-strokes with EGR

While many concepts are shared between EGR systems for the automotive four-strokes and large marine two-strokes, the two areas of control design differ considerably due to differences in two- and four-stroke scavenging, system time constants, availability to engine test stands, sensor availability and general maturity of the field. The key differences is that the two stroke scavenge (intake) manifold needs to have a higher pressure than the exhaust manifold to get fresh air into the cylinders. This necessitates the usage of a valve and a blower (pump) that can move burned gases from the exhaust manifold to the intake manifold, this pump must be combined with a valve to provide EGR shut-off and flow control for low flows. While in automotive engines the EGR flow can be produced by creating back pressure and opening an EGR valve.

The application of exhaust gas recirculation on a two-stroke cross-head diesel was published by MAN Diesel & Turbo in a number of technical reports (Pedersen et al. 2010; Kaltoft 2011; MAN Diesel & Turbo 2012; Kaltoft and Preem 2013) which mainly reported about mechanical and chemical challenges, and little on control. An MVEM of a test engine with EGR was published by Hansen, Zander, et al. (2013) along with a black-box nonlinear model identification approach. Hansen, Blanke, et al. (2013) also published a companion paper that investigated scavenge oxygen control on the basis of the MVEM. Classical feedforward and feedback designs were compared to QFT designs applied to a linearised version of the MVEM. The work only considered SISO control. Dead time of the primary sensor (scavenge gas extraction system and oxygen fraction measurement) was shown to be the main limitation of control performance. Further work on modelling the DRC test engine was published by Alegret et al. (2015). Fuel injection timing, exhaust valve timing and the cylinder bypass valve was included in the model. A Seiliger cycle was used for calculation of temperature of gas flow from cylinders and an elaborate scheme for parameter identification was presented. The operating region of the model only included the upper half of the engine load range since auxiliary blowers were not included and available maps of turbine, compressor and EGR blower performance were limited in range. Efforts to extrapolate to low load conditions where presented in (Llamas and Eriksson 2017) and (Llamas and Eriksson 2016) as part of the Hercules II project (Kyrtatos 2016). Much of the modelling efforts for building a complete dynamic ship propulsion system model with a dynamic two-stroke engine with EGR that is capable of describing the full operating region of the engine are documented in the PhD thesis (Llamas 2018).

1.1.2. The Contents and Contribution of This Paper

The adaptive feedforward (AFF) controller developed in Nielsen, Blanke, Eriksson, and Vejlgaard-Laursen (2017) showed to have a great potential to improve the acceleration performance during vessel engine testing. The interested reader is referred to the PhD thesis (Nielsen 2016) that gives a detailed treatment of EGR control in two-stroke engines. However, before the proposed solution can be adopted widely to more EGR engines, further testing has to be carried out. Since engine testing is limited by the amount of available EGR engines built and also due to high costs of vessel testing, a full vessel and EGR engine model was developed in Llamas and Eriksson (2019) to give a virtual engine and ship that can help identify potential problems during vessel manoeuvring transients.

This paper builds upon the conference paper (Llamas and Eriksson 2018). A new approach for the EGR flow controller that tracks the AFF flow setpoint output is described in this study. Moreover, the usage of the complete simulation model to analyse the controller performance is illustrated, and it identifies the low load area during ship accelerations as the most problematic case. This issue is further studied by introducing errors in the flow estimator used by the controller at low loads with the purpose to analyse the controller robustness. As a result, it is shown that sensor bias can be problematic and lead to the formation of black smoke, while parameter uncertainty has a lesser effect. Increasing the EGR blower flow capacity at low loads is also identified as a factor that has potential to improve the low load EGR control performance. The most significant contribution here is the added details on the function and properties of the actuator range splitting that was introduced in the original paper and how its nonlinear characteristic can be handled.

2. Engine and ship model

The studied container ship is powered by a MAN Diesel & Turbo uniflow two-stroke diesel engine with EGR system for Tier III operation. The engine has six cylinders with 3.45 m stroke and 0.8 m bore. At 73.9 rpm it can deliver a maximum rated power of 23 MW.

The engine is modeled following an MVEM approach (Eriksson and Nielsen 2014), where the dynamics are given by the filling and emptying of the different control volumes together with the turbocharger speed dynamics. Figure 1 contains a diagram of the modeled engine. The rectangles represent the control volumes with its corresponding states inside. The main mass flows are written in the diagram together with the control inputs. The MVEM is implemented in Simulink, and it has 41 states and 10 control inputs. Note that the mass fractions, X, contain one state for each of the four considered species, i.e. $[O_2, CO_2, H_{2O}, SO_2]$. The complete ship model is completely described, parameterised and validated using real ship measurement data in Llamas and Eriksson (2019). The model captures the stationary engine operation for a wide span of engine loads well, from 10% to 90%, both with and without the EGR system activated. The stationary relative errors are in general under 3.35% for both estimation and validation data which is a good indication of model accuracy.

3. Engine controller

The engine can operate in four distinct Engine Running Modes (ERM), depending if the secondary turbocharger

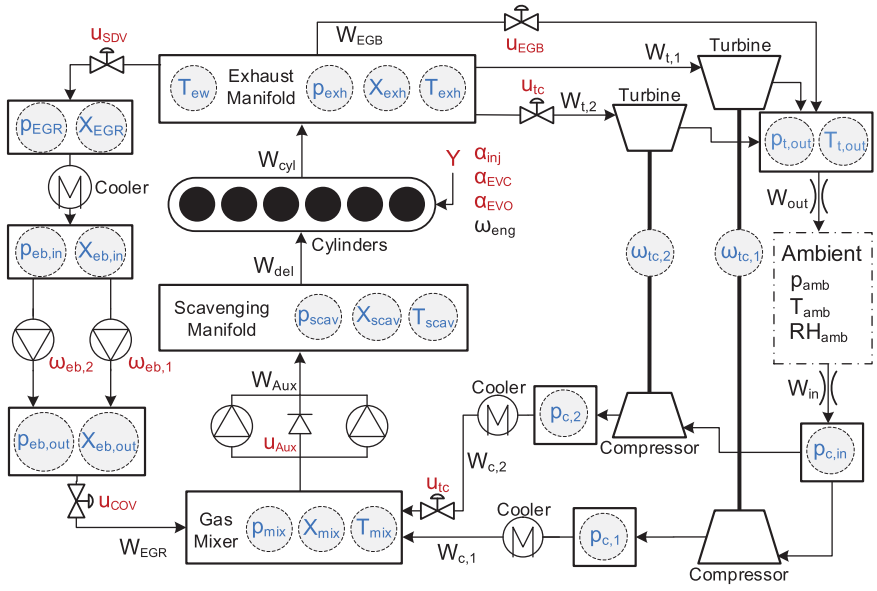

Figure 1. Modelled engine with the model states and control inputs.

is working and if one or two EGR blowers are running. Here only the fourth ERM is studied, which corresponds to both EGR blowers running and the secondary turbocharger deactivated by closing the turbo cut-out valve, u_{tc}. The EGR Shut Down Valve, u_{SDV}, is open if the engine is operating with EGR and closed otherwise. The cylinder control inputs $(\alpha_{inj}, \alpha_{EVO}, \alpha_{EVC})$ and the Exhaust Gas Bypass (EGB) valve are controlled here depending on the current ERM and Load, which may not entirely coincide with the real engine control. Finally, the auxiliary blowers are enabled and disabled if the scavenging pressure is below or above a certain value respectively. An overview of the vessel model with the speed governor, the fuel limiter and the EGR controller is shown in Figure 2. The same ordered blower speed, ω_{eb} is applied to both EGR blowers.

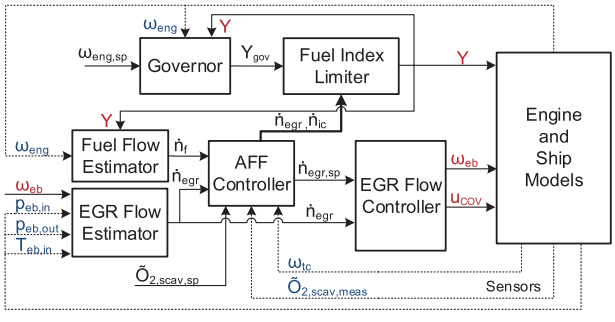

Figure 2. Diagram of the connections between the governor, the fuel index limiters, the EGR controller and the engine and ship models. The diagram shows the primary signals in solid lines and the sensors using dashed lines.

3.1. Engine speed governor

The governor controls the engine speed to follow the ordered speed setpoint by adjusting the fuel index signal, Y_{gov}. The governor is modelled as a PI controller, see Xiros (2002). During accelerations, the governor ordered fuel index is usually limited to protect the engine. To prevent the controller from winding up while its output is saturated, a tracking term is included as suggested in Åström and Hägglund (2006). The speed governor is defined as

$$Y_{gov} = K_{gov} e_\omega + \left(\frac{K_{gov}}{T_{i,gov}} e_\omega + \frac{1}{T_{t,gov}} (Y - Y_{gov}) \right) \frac{1}{s} \quad (1)$$

where e_ω is the difference between the ordered and the current engine speeds. The parameter K_{gov} is the controller gain, $T_{i,gov}$ is the integration time and $T_{t,gov}$ is the tracking time. Note that when the fuel index is not saturated, $Y = Y_{gov}$, and the tracking term in (1) is zero.

3.2. EGR controller

The EGR controller is based on molar flows, $\dot{n}$, instead of mass flows to be able to use the measured volumetric oxygen fraction directly. The AFF controller sets the current EGR flow setpoint to follow a certain oxygen reference in the scavenging manifold. The EGR flow setpoint is then tracked by the EGR flow controller to define the blower speed and Cut-Out Valve (COV) position. The different controller blocks can be seen in Figure 2. The fuel molar flow estimate $(\dot{n}_f)$ is based on a linear function of engine speed and fuel index value, more details can be found in

Nielsen, Blanke, Eriksson, and Vejlgaard-Laursen (2017). The EGR molar flow estimate ($\dot{n}_{egr}$) is based on an ellipse model, fitted to the single measured speed line using the nondimensional flow and head coefficients, Φ and Ψ respectively. The model is defined as

$$\Phi = a\left(1 - \left(\frac{\Psi}{b}\right)^n\right)^{1/n} \tag{2}$$

with tree parameters a, b and n. The nondimensional coefficients are defined as

$$\Phi = \frac{\dot{n}_{egr} T_{eb,in} R}{p_{eb,in} \omega_{eb} 4 r_{eb}^3} \tag{3}$$

$$\Psi = \frac{c_{p,eb} T_{eb,in}}{\omega_{eb}^2 r_{eb}^2} (\Pi_{eb}^{(\gamma-1)/\gamma} - 1) \tag{4}$$

where r_{eb} is the blower radius and the thermodynamical parameters $(R, \gamma, c_{p,eb})$ are taken as constants.

The key equation originally described in Nielsen, Blanke, Eriksson, and Vejlgaard-Laursen (2017) to create the feedforward part of the AFF controller is repeated here for completeness. With the following definitions

$$d = [\dot{n}_f \quad \omega_{tc}]^{\mathrm{T}}, \quad u = \dot{n}_{egr} \tag{5}$$

and simplifying the gas transport and mixing dynamics, the volumetric oxygen concentration in the scavenging manifold can be computed as

$$g(\theta, d, u) = \tilde{O}_{2,a} - \frac{(1 + \frac{y}{4}(\tilde{O}_{2,a} + 1))\dot{n}_f \dot{n}_{egr}}{(\theta\beta(\omega_{tc}) + \frac{y}{4}\dot{n}_f)(\theta\beta(\omega_{tc}) + \dot{n}_{egr})} \tag{6}$$

where $\tilde{O}_{2,a}$ is the constant molar oxygen fraction of air, y is the constant total ratio of hydrogen to carbon in the fuel. Note that some of the assumptions taken in Nielsen, Blanke, Eriksson, and Vejlgaard-Laursen (2017) to derive (6), are not fulfilled in the MVEM used here. The model structure has changed slightly, a new control volume, named gas mixer, is included in the model. The gas mixer is connected to the scavenging manifold through the auxiliary blowers. Moreover, the gas mixing dynamics in the EGR loop have been considered including three control volumes. Furthermore, the coolers contain models for the Water Mist Catchers (WMC). Its main function is to remove the condensed water in the flows, and thus they alter the oxygen concentrations slightly.

The molar flow delivered by the main compressor cooler is computed as

$$\dot{n}_{ic} = \theta\beta(\omega_{tc}) \tag{7}$$

where $\beta(\omega_{tc})$ is a second order polynomial of the turbocharger speed. The parameter θ is adjusted with the adaptation algorithm from Nielsen, Blanke, and Eriksson (2017) that guarantees oxygen setpoint convergence. The adaptation law is defined as

$$\dot{\hat{\theta}} = k\left(\tau\dot{\tilde{O}}_{2,scav,meas+} \int \tilde{O}_{2,scav,meas} - g(\hat{\theta}, d, u)\,\mathrm{d}t\right) \tag{8}$$

with $k > 0$, and the sensor and gas mixing dynamics represented by τ. The adaptation uses the oxygen measurement together with the model for the scavenging oxygen concentration (6), to update $\hat{\theta}$. Finally, the EGR molar flow setpoint, $\dot{n}_{EGR,sp}$, is obtained by inverting (6), based on the current molar flow estimates and the desired oxygen concentration setpoint. Convergence proofs for exponential convergence of both the estimator and controller in the AFF are shown in Nielsen, Blanke, Eriksson, and Vejlgaard-Laursen (2017). The paper also shows experimental results of the AFF controller operating in a container ship.

A new EGR flow controller that tracks the EGR flow setpoint is introduced in this study. In normal operation, the blower speed is used to control the EGR flow. If the lower blower speed limit is reached, the COV valve is used to reduce the flow further until the blower speed can retake control. To avoid controllability problems, a single PI controller is used to control both actuators using a split-range control approach, see Åström and Hägglund (2006). The static relationship between the PI controller output and the actuated signals is depicted in Figure 3. The blower speed limits are constant values, the maximum valve position is 1, and $u_{cov,\min}$ depends on the current engine load. The PI controller is defined as

$$v = K_{egr}\, e_{\dot{n}} + \left(\frac{K_{egr}}{T_{i,egr}} e_{\dot{n}} + \frac{1}{T_{t,egr}}(u_{pid} - v)\right)\frac{1}{s} \tag{9a}$$

$$u_{pid} = \max(-0.5, \min(v, 1)) \tag{9b}$$

where the error, $e_{\dot{n}}$, is the difference between the EGR molar flow setpoint and the estimated flow. The PI controller output, u_{pid}, is limited to the defined controller range $[-0.5, 1]$, see Figure 3. Due to this output saturation, the PI controller contains an anti-windup term

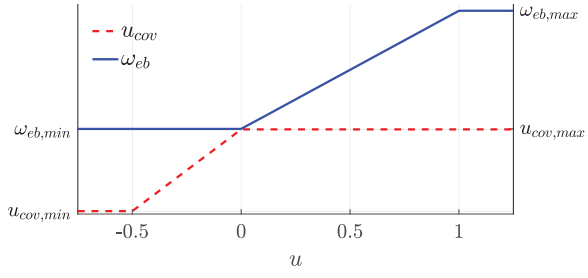

Figure 3. Split-range control diagram of the two actuator outputs depending on the PI controller output.

with constant tracking value $T_{t,egr}$, as in (1). Quicker and wider changes in the actuated signals are required at low engine loads. To obtain good controller performance, the PI gain is scaled to have larger gains at low loads using the scavenging pressure signal as follows

$$K_{egr} = \frac{K}{p_{scav} \cdot 10^{-5}} \tag{10}$$

with the pressure in *Pa*. Then, K and $T_{i,egr}$ are fixed constant values. The actuator outputs are calculated using the limits as

$$\omega_{eb} = \frac{\omega_{eb,\max} - \omega_{eb,\min}}{1} \max(0, u) + \omega_{eb,\min} \tag{11a}$$

$$u_{cov} = \frac{u_{cov,\max} - u_{cov,\min}}{0.5} \min(u, 0) + u_{cov,\max} \tag{11b}$$

The PID controller signal can now be fed into this range splitting function

$$u = u_{pid} \tag{12}$$

The asymmetry in the defined control range between both actuators has the purpose of establishing suitable control gains for each actuator, e.g. the blower speed gain from the flow error, $e_{\dot{n}}$, is substantially larger due to the speed units compared to the valve normalised position.

3.2.1. Nonlinear Compensation for the Valve Characteristics

A sequence of EGR actuator sweeps from minimum to maximum control at constant engine speeds (i.e. the same as constant ship speeds) have been performed to analyse the behaviour of the switching controller. The sweeps starts from closed COV and crosses over to maximum blower speeds, where it ends, which means that it goes from low to high EGR flows. The results are presented with the control input u_{pid} on the x-axis and a 'normalized EGR flow' which is the EGR flow $\dot{n}_{egr}(u)$ scaled with the inverse of the flow at control input of 0, i.e. $\dot{n}_{norm}(u) = \dot{n}_{egr}(u)/\dot{n}_{egr}(0)$. The results are shown in the top left plot in Figure 4, where one can see three distinct responses plus a twitch. To the left (i.e. $u_{pid} < 0$) the EGR cut out valve is active while to the right (i.e. $u_{pid} > 0$) the EGR blower is active. The right side of the plots have

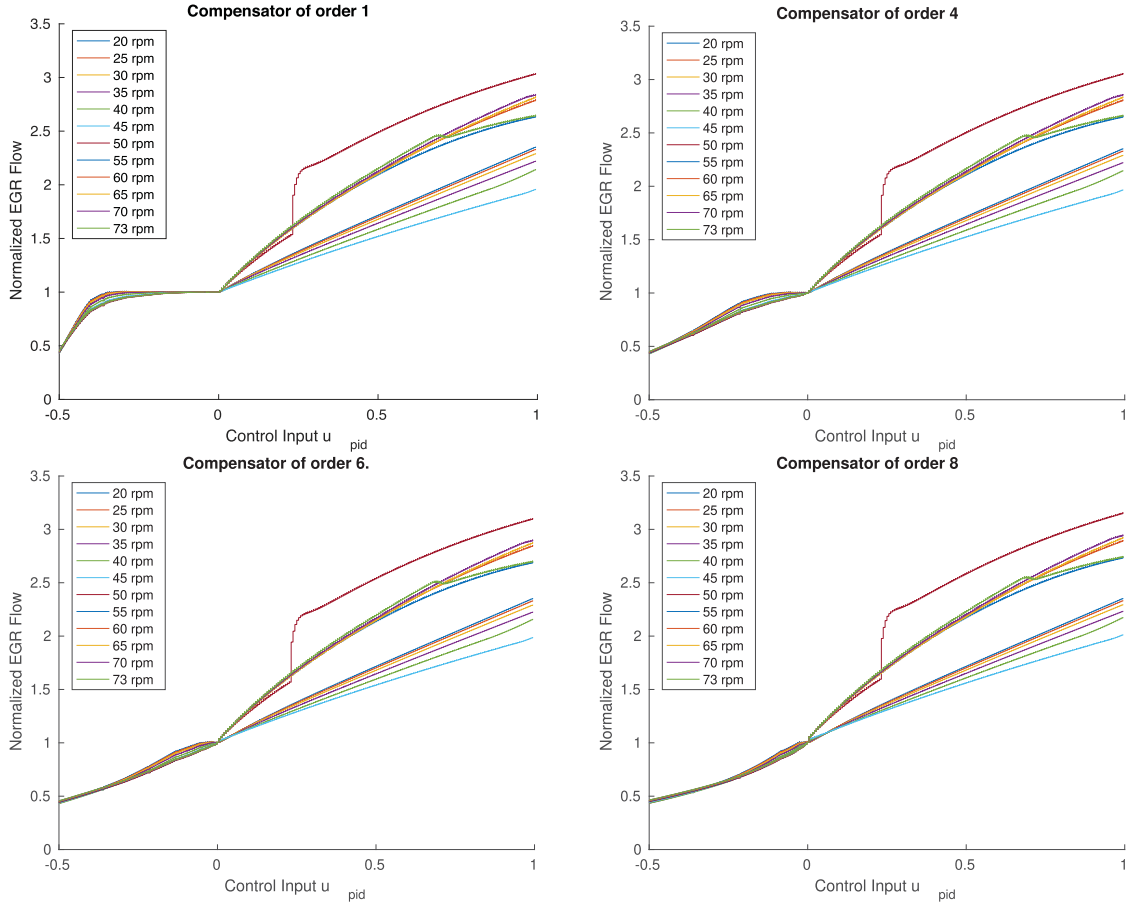

Figure 4. Example of nonlinear connection between achieved EGR-flow and control action u_{pid}. The **top left** describes the standard connection between the PID output and the normalised EGR. The other plots display what happens when the control action for the COV is changed using a non linear transformation defined in (13).

identical responses as the EGR blower is operated in the same way in all four cases. Concentrating on these ones to the left the 6 lowest responses correspond the engine speeds in the range 20–45 RPM, with 20 giving the highest EGR at $u_{pid} = 1$. For the next speed 50 RPM (which is the one with a twitch) the engine starts with a high scavenging manifold pressure so the auxiliary blower is off, as the amount of EGR increases the boost pressure is reduced and the pressure reaches the limit where the auxiliary blower is turned on. This increases the EGR drawn through the systems and results in the jolt of EGR at $u_{pid} \approx 0.25$. For the rest of the speeds the blower is off and the responses are more smooth. For the highest requested speed the added EGR causes a reduction in the available air and the engine speed cannot be maintained by the governor. That causes the drop in the final speed curve (72 RPM) at $u_{pid} \approx 0.7$.

The behaviour for the case when the EGR blower is running at minimum speed and the COV is opened linearly is seen in the top left plot of Figure 4. There one sees that not much happens with the EGR for $u_{pid} \in [-0.3, 0]$ which is due to the throttle area and pressure characteristics. This behaviour can be mitigated by applying a nonlinear transformation to the control signal in the following way

$$u = \begin{cases} u_{pid} & \text{if } u_{pid} \geq 0 \\ -0.5\sqrt[n]{-2\,u_{pid}} & \text{if } u_{pid} < 0 \end{cases} \tag{13}$$

where the value of n in the nth root, that controls the shape of the nonlinearity. (13) replaces (12) and is fed to the actuator range splitting function (11) graphically illustrated in Figure 3, and the resulting control action is illustrated in Figure 5 for $n \in [1, 4, 6, 8]$. The figure shows how the shape of the nonlinear compensator changes the COV characteristics and how it depends on the order of the root, where $n = 1$ corresponds to the original function. The impact that the transformation (13) has on the relation between the PID control output and EGR in the engine is shown in the three plots to the right and bottom of Figure 4. As the figures show it is the one with $n = 6$ that most closely mimics a linear behaviour. This is a desirable property since the system gain is most repetitive over the operating region this makes it easier to select a suitable control gain that can give a good response over the operating region.

3.3. Fuel index limiters

The injected mass flow is usually limited in various operating situations to prevent engine damage. This is done by specifying an upper value to the fuel index signal, see Xiros (2002). A new Dynamic Limiter Function (DLF), has been developed at MAN Diesel & Turbo, see Vejlgaard-Laursen and Olesen (2016), to ensure better acceleration capacity of vessels with downsized engines. This limiter consists of two parts, one that limits the maximum amount of fuel based on an estimate of the trapped air mass in the cylinders and a lower lambda limit, Y_{LA}, and another that limits the fuel to protect the engine from too extreme torsional vibrations, Y_Q. The DLF also controls the injection and exhaust valve timings for faster transients. However, this is not implemented in this paper but could be included by defining specific control laws for α_{inj}, α_{EVC}, and α_{EVO}.

For engines with EGR, the oxygen concentration is lower since the recirculated exhaust gas replaces some of the fresh air in the scavenging receiver. Hence, the amount of fuel that can be burned during accelerations depends not only on the trapped mass but also on the oxygen concentration of that mass. A correction needs to be applied to Y_{LA} to prevent the engine of producing black smoke from incomplete combustion. The oxygen/fuel limiter, Y_{LOM}, described in Nielsen et al. (2018), does this correction by making use of the scavenge oxygen equation (6) to correct the DLF limiter when EGR is being used. Thus, the ordered fuel index going to the engine is calculated as

$$Y = \min(Y_{gov}, Y_{LOM}, Y_Q) \tag{14}$$

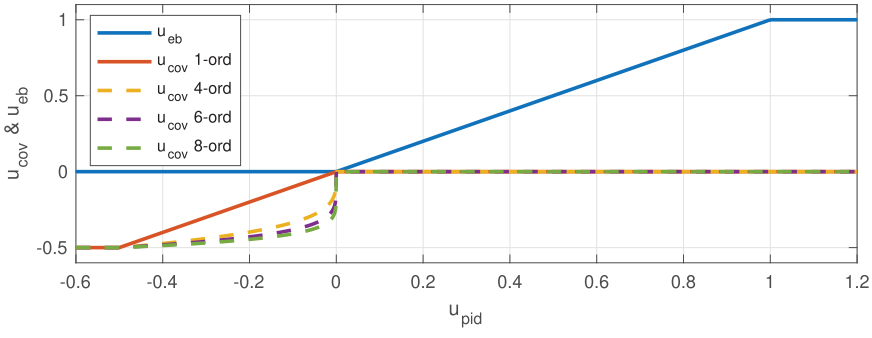

Figure 5. Examples of how the shape of the nonlinear compensator changes the COV control characteristics and how it depends on the order of the root.

4. Results

In Section 4.1 the governor and EGR controller are investigated under different scenarios to analyse its performance. Moreover, in Section 4.2 the controller robustness is also examined by adding disturbances to the flow estimators inputs and parameters. The standard controller without actuator compensation are used in Sections 4.1 and 4.2. The nonlinear actuator compensation is analysed in Section 4.3. The analysis ends with a short discussion, in Section 4.4, about the direct benefits of having a versatile and suitable simulation model.

4.1. Acceleration scenarios

Three consecutive increasing engine speed steps have been simulated, the main signals and controlled inputs are shown in Figure 6. These speed steps correspond to engine load increases from 9% to 90%. After an initial transient, the oxygen level converges to the desired setpoint for all steps. The convergence is connected to the adaptation parameter, $\hat{\theta}$, and it is achieved once a stable value is reached. The bottom plot of Figure 6 shows

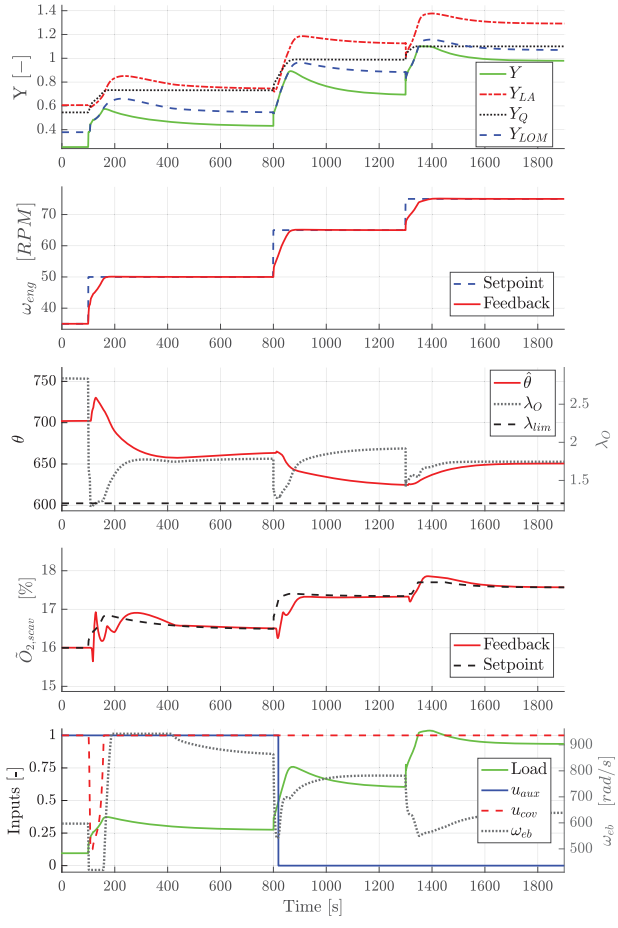

Figure 6. EGR and fuel controller performance during three consecutive engine speed steps.

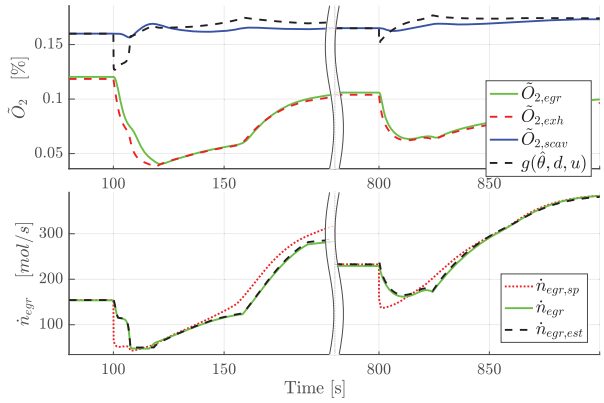

Figure 7. Oxygen Dynamics and EGR molar flows during the two first engine speed steps from Figure 6.

the EGR control inputs and the engine load. For the first speed step, the blower speed reaches its lower limit, and the COV valve has to be actuated to reduce the flow. The lowest speed step also has the largest oxygen setpoint deviation at the start of the step, initially drops under 16% and when the COV valve is actuated it crosses the setpoint. After that, the blower speed has to be increased again until it reaches its limit, this shows that EGR blowers with larger flow capacity at low loads would improve the controller performance.

This fast overshoot in the first step is a direct consequence of the quick feedforward setpoint change. The feedforward is built by simplifying the model dynamics and thus assumes that changes in the exhaust flow concentrations have a rapid impact on the scavenging concentration. This takes a long time at low loads due to the slower turbocharger dynamics. This issue can be observed in the zoom-ins of the first two steps shown in Figure 7. The model from (6) predicts a quick oxygen drop in the first step due to the rapid fuel flow increase. If the corresponding EGR flow setpoint was followed perfectly, the overshoot in the oxygen value would be even larger, as can be seen in Figure 8 for the baseline case. Once the adaptive parameter starts to be influenced by the delayed oxygen measurement, the oxygen value reaches the setpoint. For the second load step, this issue is not as critical as can be seen on the right side of Figure 7. However, this behaviour at low loads could be problematic if, for example, the flow estimates are biased, which is further investigated in the next section.

4.2. Controller robustness simulations

The first speed step from the previous section is first investigated by biasing the EGR flow input signals. Results with a 3% increase and decrease on the inlet pressure together with band limited white noise added to the

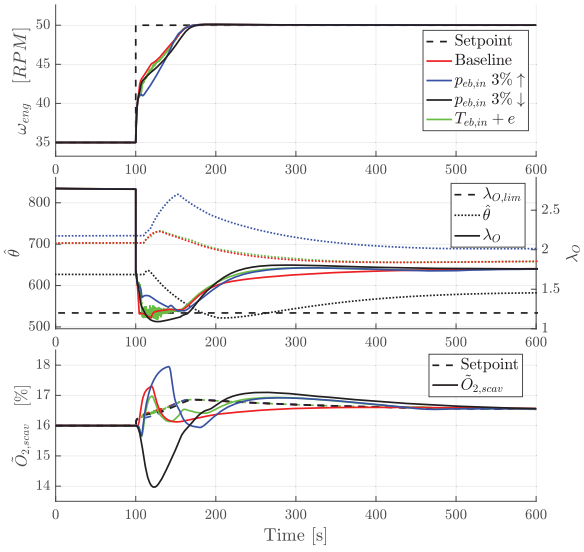

Figure 8. Low load speed step results for disturbances in the inlet pressure of the EGR flow estimator and noise added to the inlet temperature of the EGR blower.

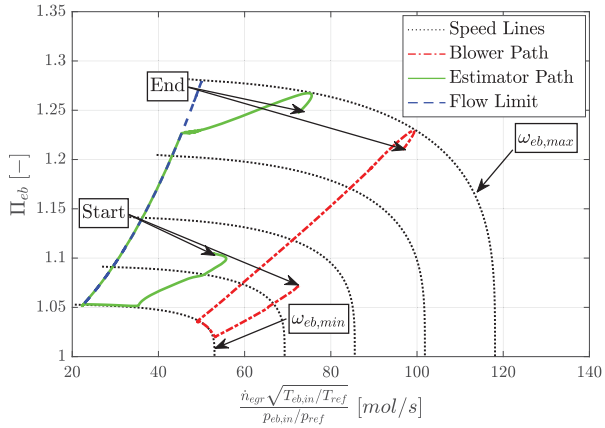

Figure 9. Real blower and flow estimator operating paths in the pressure ratio vs corrected molar flow plane. It corresponds to the $p_{eb,in}$ 3% ↓ case from Figure 8.

blower inlet temperature signal are shown in Figure 8. The added noise is exaggerated by using a standard deviation of 10 K. Figure 8 also contains, as a baseline, the case without EGR blower speed limits so that it is easier to compare what would be the best case. The first issue that can be observed is that for the noisy temperature signal, the performance is not substantially reduced. The worst implication is that the fuel index limit calculation is affected by the noise in the EGR flow estimate which results in the lambda value crossing the limit. Similar results have been observed by applying noise to the blower pressure signals, and in all cases, the issue can be prevented with an appropriate filter. The biased pressure cases show more interesting results. With a higher measured inlet pressure, the controller overestimates the EGR flow. This produces an overshoot in the oxygen value and a slightly slower acceleration in the beginning due to a more restrictive fuel limiter.

On the other hand, with a lower measured inlet pressure, the results are the opposite. The EGR flow estimator is working with higher pressure ratios which correspond to an underestimate of the EGR flow. The controller initially expects the oxygen to be higher due to the low EGR flow, which results in a lower oxygen concentration together with a lambda that crosses the limit value. The blower response along with the estimator are shown in Figure 9, where it is seen that a 3% decrease in inlet pressure moves the operating path of the estimator substantially due to the relatively flat blower speed lines in this region. To avoid that the estimator ends up at zero flow, which would have even worse implications for the control performance, a lower flow limit is used in the estimator. The limit is implemented as a saturation of the head parameter, see (15), before evaluating equation (2), and it is depicted in Figure 9 in the pressure ratio-corrected flow plane.

$$\Psi = \min(0.99 \cdot b, \Psi) \tag{15}$$

Similar results as those described above are obtained when biasing the other flow estimator input signals, however, to get similar oxygen deviations, the bias in the blower inlet temperature or turbocharger speed has to be substantially larger than 3%. For the case of blower outlet pressure, similar results are obtained since it influences the pressure ratio and thus moves the operating point of the blower in the same manner as the inlet pressure case. The simulations also show that the sensor bias undesired effects can be significantly reduced by changing either the inlet or the outlet absolute pressure sensor for a differential pressure sensor type. Then, the unmeasured inlet or outlet pressure is computed with the remaining absolute pressure sensor signal plus or minus the measured differential pressure. With this measurement setup, a much higher bias than 3% is required to reach the same undesired effect, which should not happen in the real controller setup.

Further investigations are carried out by modifying the parameters of the flow estimate models. The fuel flow model parameters are increased and decreased by 15% to obtain both over and underestimation of the fuel flow. The EGR flow estimate model is used with the parameters corresponding to the most closed and the most open blower diffuser positions. Closing the blower diffuser vanes results in less flow, and opening them has the contrary effect. Note that the diffuser position in the engine model is fixed at the middle position. Results are shown in Figure 10. As can be observed, the oxygen deviation from the setpoint is less pronounced than for the

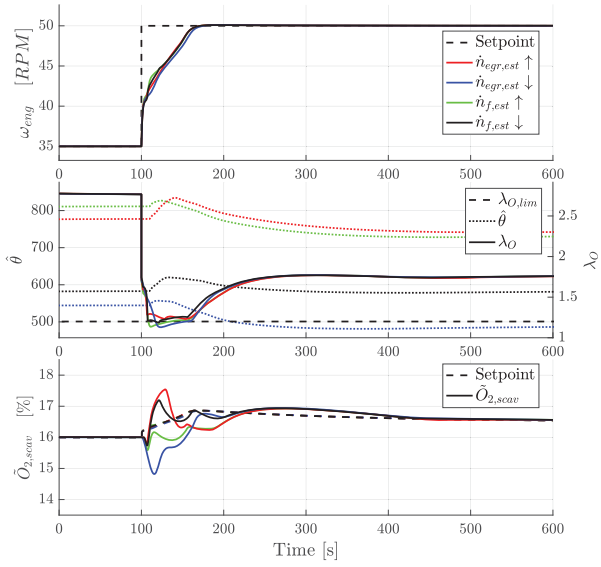

Figure 10. Low load speed step results for under and overestimation of EGR and fuel flows in the EGR controller.

previous case where the $p_{eb,in}$ was biased. All four cases have little effect on the in-cylinder lambda value, which remains quite similar. This is a valuable result because, in the real application, it can be difficult to verify whether or not the parameters of the flow estimators are accurate. When the EGR controller is calibrated for a new engine, tuning the EGR estimator from the manufacturer EGR blower map and the fuel estimator from stationary fuel consumption measurements during the engine shop test should be sufficient to obtain a good performance.

4.3. Sequence of acceleration steps and COV impact

A sequence of steps have been performed on the complete ship simulation model, with all engine controllers related to operating mode 4 activated, this is done in order to investigate the properties of the system and the control performance of the Cut-Out Valve (COV) u_{cov}. The steps are shown in the top plot of Figure 11, and they cover the complete speed region of the engine model.The top shows the setpoint and achieved engine speeds, the middle shows the EGR blower speed, and bottom plot shows EGR cut out valve (COV) together with the auxiliary blower that turns off at 4500 seconds. As a side note the capacity of the engine is exceeded when requesting 80 RPM, so the engine cannot reach 80 RPM. This step is removed

The engine speed step responses are shown in Figure 12. To make the step responses, shown in the previous figure, comparable, all steps are shifted so they start at 20 RPM and we study 10 s. It is seen that the response time increases with engine (and ship) speed. This engine speed response is a reaction on the fuelling through the engine dynamics connected to the powertrain with propeller and ship dynamics.

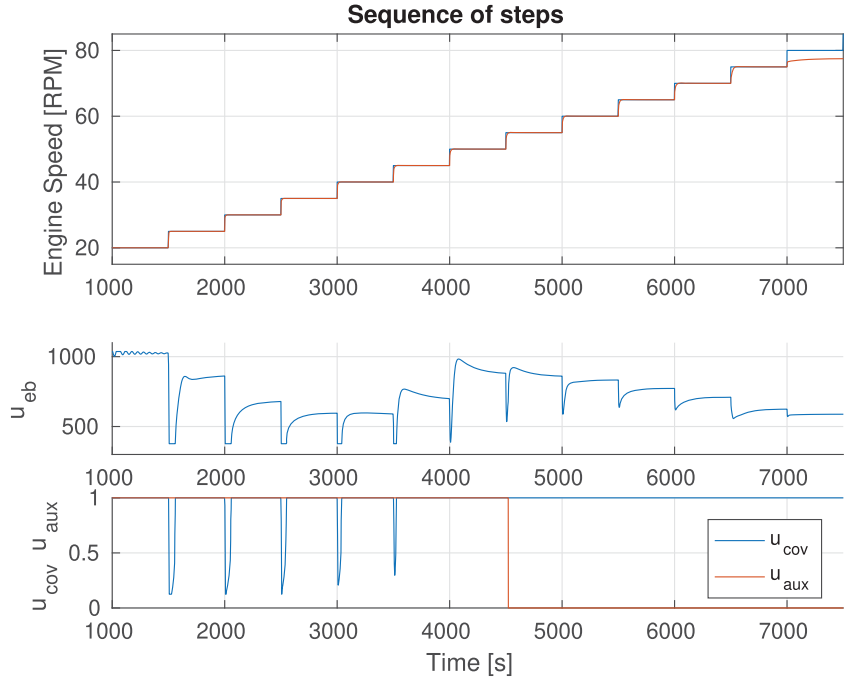

Figure 11. A sequence of steps in reference engine speed that ramps over the engine speed range with 5 RPM changes each time. The **top** plot shows the engine speed. The **mid** plot shows the EGR blower speed. The **bottom** plot shows the COV valve operation and the. It is in the lower speed range where the u_{cov} becomes active, especially the first 5 steps cause the COV valve to close. These will be studied in more detail later.

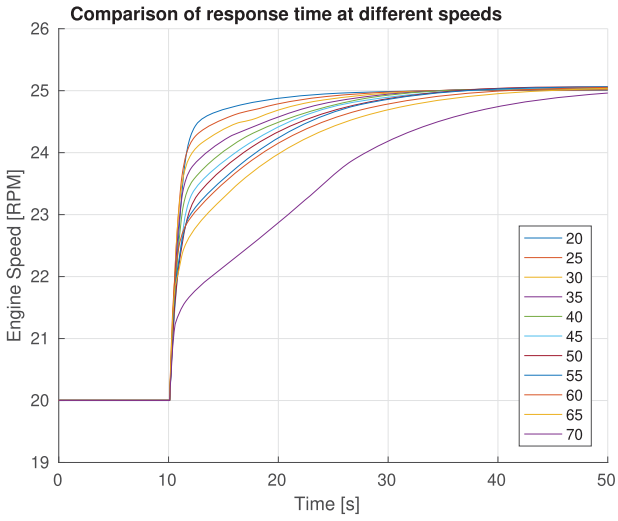

Figure 12. Speed steps from Figure 11 adjusted to make comparisons easy, by subtracting an offset so all start at 20 RPM. The response time for the engine speed increases with engine (and ship) speed.

The impact of the COV control is, of course, only visible when the COV is active which it is in transients for the first 5 steps in Figure 11. Therefore, these steps are studied in more detail in Figures 13 and 14 that show the standard controller (12) and the transformed controller (13) with $n = 6$, respectively. For the standard controller Figure 13, one can see a bump in the O_2 responses during the decay phase, this comes from the control action when the COV actuator traverses the flat region for negative u_{pid}, i.e. control signals corresponding to $u \in [-0.3, 0]$

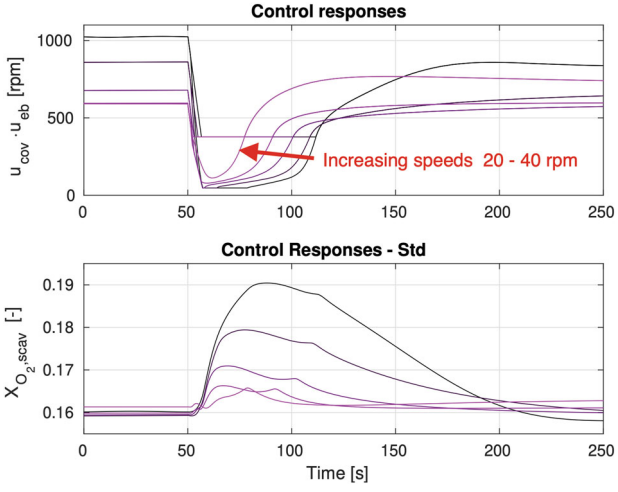

Figure 13. Response in Scavenge receiver oxygen concentration for the 5 steps at lowest speeds where the COV valve is active during the steps. This is for the standard controller without the actuator compensation. A bump is seen in the O_2 responses during the decay phase, this comes from the phase when the COV actuator traverses the flat region for negative u_{pid} the left in the top left plot of Figure 4.

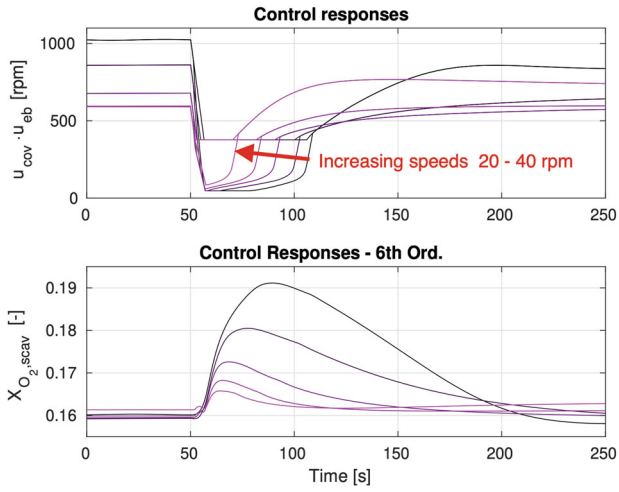

Figure 14. Response in Scavenge receiver oxygen concentration for the 5 steps at lowest speeds where the COV valve is active during the steps. This is for the nonlinear controller of order 6.

producing a flat region to the left in the top left plot of Figure 4.

When the nonlinear transformation (13) is employed, as in Figure 14, the bump is reduced significantly.

The only small residual of a bump, is due to the rate limiter (slew rate) that is present in the actuator. This is due to the nonlinearity acting on u_{pid} which causes u to change rapidly near $u = 0$, and the actuator lags behind slightly. Anyway, the bump is significantly improved, and the response exhibits a smooth behaviour.

As side comment it is interesting to note that the torque build-up dynamics is slower for high speeds while the gas flow and mixing dynamics in the volumes are slower for low speeds. The latter is due to the fact that low loads have lower mass flows with which it takes a longer time to fill the volumes with mass and change mixture strengths. At higher speeds the flows are relatively higher and fills the volumes quicker but the ship resistance is also higher which causes the vessel dynamics to be slower.

4.4. Savings obtained using the model

It is more of a curiosity but the cost reduction in the control development, achieved from using a model, has been estimated in the following way. The engine and ship model constitute a digital twin to the ship for which it was built to mimic. If the tests performed to study the system had been performed on the real engine and ship, fuel would have been consumed as well as engineering hours. As a measure of the resources needed the simulation results that records traces of fuel usage, vessel speed and time, have been used to compute the fuel, distance, and time. The data collected from the simulation results show the following experimental facts:

```
Total Fuel Saved : 360 ton (metric)
Sailing Time Saved : 260 hours
Sailing Distance Saved : 6000 km
```

These only represent a bare minimum of experiments on the virtual ship that were needed to generate the results, in reality the development consumed more than double the amount of simulations. If we were performing tests with a real ship we might also have missed some aspects that needed to be remade, but we would think more carefully if we were dealing with costly real-world resources. Anyway we can see the numbers as reasonable approximations of how much the digital twin can save in development cost. Another facet that is worth to mention is, the testing has been performed in conditions that are far from optimal and could have generated much more NO_x and particulates than the ship would in nominal operation, which is also a benefit of the virtual development.

5. Conclusions

The AFF controller together with the proposed EGR flow controller is shown to perform well during ship acceleration simulations at different loads. Having EGR blowers with more flow capacity at low loads would be useful for improving the oxygen control performance since the controlled speed hits the lower and upper limits. Moreover, it has been identified that simplifying the dynamics of the AFF inverted model has a substantial impact at low loads where the engine air path dynamics are slower. If the controller flow estimates are accurate, this issue does not impact the control performance substantially. However, when sensor bias is introduced to the EGR blower inlet pressure, the controller performance is affected due to the shift in the operating region of the EGR flow estimate model. This is identified as the most sensitive case, since underestimating the EGR flow could lead to the formation of black smoke during the acceleration. This undesired effect can be prevented by proper sensor calibration or by using a differential pressure sensor in combination with an absolute pressure sensor in the EGR flow estimator. On the other hand, the simulations show that errors in the parameters of the fuel and EGR flow estimators have a lesser effect on the oxygen tracking performance. This is an important result since correctly parameterising the flow estimators could be difficult for a given engine.

It has also been shown how an actuator nonlinearity in the EGR cut out valve COV can be mitigated using a nonlinear transformation. Finally, a quantification is given for how much resources (fuel and time) the development would have consumed if real world experiments would have been performed instead of simulations.

Nomenclature and abbreviations

AFF	adaptive feed forward
c_p	specific heat at constant pressure
e	error
COV	cut out valve
DLF	dynamic limiter function
EGR	exhaust gas recirculation
EGB	exhaust gas bypass
ERM	engine running mode
MVEM	mean value engine model
$\dot{n}$	molar flow
NECA NO_x	emission control areas
$\tilde{O}_2$	oxygen molar fraction
p	pressure
P	power
PI	proportional and integral controller
PID	proportional, integral, and derivative controller
R	gas constant
r	radius
T	temperature
u	input signal
VGT	variable geometry turbine
W	mass flow
WMC	water mist catcher
X	mass fraction
Y	fuel index
Y_{LA}	fuel limiter using air
Y_Q	fuel Limiter reducing the torque
Y_{LOM}	fuel limiter using oxygen model
Greek symbols	
α	crank angle
γ	specific heats ratio
ω	rotational speed
Φ	dimensionless flow coefficient
Π	pressure ratio
Ψ	dimensionless head coefficient
$\hat{\theta}$	adaptive parameter
λ_o	oxygen to fuel ratio
Subscripts	
a	air
aux	auxiliary blower
c	compressor
cov	cut-out valve
cyl	cylinder
eb	EGR blower
eng	engine
est	estimated

exh	exhaust
f	fuel
gov	governor
ic	air cooler
in	inlet
inj	injection
meas	measured
out	outlet
pid	PID controller
ref	reference
scav	scavenging
sp	setpoint
tc	turbocharger

Acknowledgments

MAN Energy Solutions and in particular Kræn Vodder Busk are greatly acknowledged for the suggestions and for the help in setting up the EGR controller.

Disclosure statement

The authors declare that there is no potential conflict of interest.

Funding

Parts of this project has received funding from the European Union's Horizon 2020 research and innovation programme under grant agreement No 634135. Parts of this work was supported by Vinnova Competence Center for industry-academia cooperation LINK-SIC https://liu.se/en/research/link-sic.

ORCID

Lars Eriksson http://orcid.org/0000-0001-8646-8998
Xavier Llamas http://orcid.org/0000-0002-1584-8165

References

Alegret G, Llamas X, Vejlgaard-Laursen M, Eriksson L. 2015. Modeling of a large marine two-stroke diesel engine with cylinder bypass valve and EGR system. IFAC-PapersOnLine. 48(16):273–278. 10th IFAC Conference on Manoeuvring and Control of Marine Craft.

Ammann M, Fekete NP, Guzzella L, Glattfelder AH. 2003. Model-based control of the VGT and EGR in a turbocharged common-rail diesel engine: theory and passenger car implementation. In: SAE Technical Paper 2003-01-0357. SAE International.

Åström KJ, Hägglund T. 2006. Advanced PID control. ISA - Instrumentation, Systems, and Automation Society. ISBN: 978155617-9426.

Banning R, Johnson MA, Grimble MJ. 1997. Advanced control design for marine diesel engine propulsion systems. ASME J Dyn Sys Meas Control. 119(2):167–174.

Blanke M, Andersen JA. 1984. On modelling large two stroke diesel engines: new results from identification. In: Proc. IFAC World Congress; Budapest. Pergamon Press. p. 2015–2020.

Eriksson L, Nielsen L (2014). Modeling and control of engines and drivelines. John Wiley & Sons.

Guan C, Theotokatos G, Chen H. 2015. Analysis of two stroke marine diesel engine operation including turbocharger cut-out by using a zero-dimensional model. Energies. 8(6):5738–5764.

Guan C, Theotokatos G, Zhou P, Chen H. 2014. Computational investigation of a large containership propulsion engine operation at slow steaming conditions. Appl Energy. 130:370–383.

Guzzella L, Onder CH (2010). Introduction to modeling and control of internal combustion engine systems. Springer.

Hansen JM, Blanke M, Niemann HH, Vejlgaard-Laursen M. 2013. Exhaust gas recirculation control for large diesel engines - achievable performance with SISO design. IFAC-PapersOnLine, Elsevier Science. 46(33):346–351. IFAC Proceedings Volumes.

Hansen JM, Zander CG, Pedersen N, Blanke M, Vejlgaard-Laursen M. 2013. Modelling for control of exhaust gas recirculation on large diesel engines. 9th IFAC Conference on Control Applications in Marine Systems, Osaka, Japan .

Hendricks E. 1986. Compact, comprehensive model of large turbocharged, two-stroke diesel engines. SAE Technical Paper Series.

Heywood JB (1988). Internal combustion engine fundamentals. McGraw-Hill.

International Maritime Organization. 2013. Marpol: Annex VI and NTC 2008, 2013: with guidelines for implementation. London, UK: IMO.

Jankovic M, Jankovic M, Kolmanovsky I. 2000. Constructive Lyapunov control design for turbocharged diesel engines. IEEE Trans Control Syst Technol. 8(2):288–299.

Jankovic M, Kolmanovsky I. 2009. Delay differential equations: recent advances and new directions. Springer US. chapter, Developments in control of time-delay systems for automotive powertrain applications; p. 55–92.

Kaltoft J. 2011. Tier III EGR for large 2-stroke man B&W diesel engines. In: Proceedings of the International Symposium on Marine Engineering, Kobe, Japan.

Kaltoft J, Preem M. 2013. Development of integrated EGR system for two-stroke diesel engines. In: 27th CIMAC World Congress on Combustion Engine, Shanghai, China.

Kyrtatos NP. 2016. From hercules A-B-C to Hercules-2: cutting edge R&D in ship engines. Trans Res Proc. 14: 1581–1590.

Llamas X. 2018. Modeling and control of EGR on marine two-stroke diesel engines [dissertation]. Linköping University.

Llamas X, Eriksson L. 2016. A model of a marine two-stroke diesel engine with EGR for low load simulation. In: 9th EUROSIM Congress on Modelling and Simulation; Oulu, Finland.

Llamas X, Eriksson L. 2017. Parameterizing compact and extensible compressor models using orthogonal distance minimization. ASME J Gas Turb Pwr. 139(1). doi:10.1115/1.4034152

Llamas X, Eriksson L. 2018. Robustness analysis of the next generation of EGR controllers in marine two-stroke diesel engines. In: International Ship Control System Symposion, iSCSS 2018; October 2–4; Glasgow, UK.

Llamas X, Eriksson L. 2019. Control-oriented modeling of two-stroke diesel engines with EGR for marine applications.

Proc Inst Mech Eng M. 233(2):551–574. doi:10.1177/1475090218768992

MAN Diesel & Turbo. 2012. Tier III two-stroke technology; Technical paper. http://marine.man.eu/two-stroke/technical-papers.

Nielsen KV. 2016. Exhaust recirculation control for reduction of NO_x from large two-stroke diesel engines [dissertation]. Technical University of Denmark.

Nielsen KV, Blanke M, Eriksson L. 2017. Adaptive observer for nonlinearly parameterized hammerstein system with sensor delay–applied to ship emissions reduction. IEEE Trans. Control Syst. Technol. 26(4):1508–1515. doi:10.1109/TCST.2017.2715004.

Nielsen KV, Blanke M, Eriksson L, Vejlgaard-Laursen M. 2017. Adaptive feedforward control of exhaust recirculation in large diesel engines. Control Eng Pract. 65:26–35.

Nielsen KV, Blanke M, Eriksson L, Vejlgaard-Laursen M. 2017. Control-oriented model of molar scavenge oxygen fraction for exhaust recirculation in large diesel engines. ASME J Dyn Sys Meas Control. 139(2). doi:10.1115/1.4034750

Nielsen KV, Blanke M, Eriksson L, Vejlgaard-Laursen M. 2018. Marine diesel engine control to meet emission requirements and maintain maneuverability. Con. Eng. Pra. 76(June):12–21. doi:10.1016/j.conengprac.2018.03.012

Nieuwstadt M, Kolmanovsky I, Moraal P, Stefanopoulou A, Jankovic M. 2000. EGR-VGT control schemes: experimental comparison for a high-speed diesel engine. IEEE Control Systems Mag. 20(3):63–79.

Pedersen MF, Andreasen AA, Mayer S. 2010. Two-stroke engine emission reduction technology: state-of-the-art. Bergen, Norway: CIMAC Congress.

Poloni T, Rohal-Ilkiv B, Johansen TA. 2014. Mass flow estimation with model bias correction for a turbocharged diesel engine. Control Eng Pract. 23(1):22–31.

Stefanopoulou A, Smith R. 2000. Maneuverability and smoke emission constraints in marine diesel propulsion. Control Eng Pract. 8(9):1023–1031.

Theotokatos G. 2010. On the cycle mean value modelling of a large two-stroke marine diesel engine. Proc Inst Mech Eng M. 224(3):193–206.

Theotokatos G, Tzelepis V. 2015. A computational study on the performance and emission parameters mapping of a ship propulsion system. Proc Inst Mech Eng M. 229(1):58–76.

Tschanz F, Amstutz A, Onder CH, Guzzella L. 2013. Feedback control of particulate matter and nitrogen oxide emissions in diesel engines. Control Eng Pract. 21(12):1809–1820.

Vejlgaard-Laursen M, Olesen H. 2016. Controlling tier III technologies. In: 28th CIMAC World Congress on Combustion Engine, Helsinki, Finland.

Wahlström J, Eriksson L. 2011a. Modelling diesel engines with a variable-geometry turbocharger and exhaust gas recirculation by optimization of model parameters for capturing non-linear system dynamics. Proc Inst Mech Eng D. 225(7):960–986.

Wahlström J, Eriksson L. 2011b. Nonlinear EGR and VGT control with integral action for diesel engines. Oil Gas Sci Technol Rev IFP. 66(4):573–586.

Wahlström J, Eriksson L. 2013. Output selection and its implications for MPC of EGR and VGT in diesel engines. IEEE Trans Control Syst Technol. 21(3):932–940.

Wahlström J, Eriksson L, Nielsen L. 2010. EGR-VGT control and tuning for pumping work minimization and emission control. IEEE Trans Control Syst Technol. 18(4):993–1003.

Winterbone DE, Jai-In S. 1991. The application of modern control theory to a turbocharged diesel engine powerplant. Proc Inst Mech Eng I. 205(1):69–83.

Woodward JB, Latorre RG. 1985. Modeling of diesel engine transient behavior in marine propulsion analysis. Trans Soc Naval Arch Marine Eng. 92:33–49.

Xiros N (2002). Robust control of diesel ship propulsion. London: Springer-Verlag.

Xiros NI, Theotokatos G. 2011. Improved transient control of a two-stroke marine diesel engine with variable geometry turbine. In: ASME 2011 Internal Combustion Engine Division Fall Technical Conference; West Virginia, USA.

Yildiz Y, Annaswamy A, Kolmanovsky IV, Yanakiev D. 2010. Adaptive posicast controller for time-delay systems with relative degree $n \leq 2$. Automatica. 46(2):279–289.

Zhao J, Wang J. 2013. Effect of exhaust gas recirculation on biodiesel blend level estimation in diesel engines. J Dyn Syst Meas Control-Trans ASME. 135(1):011010.

Zhao J, Wang J. 2015. Adaptive observer for joint estimation of oxygen fractions and blend level in biodiesel fueled engines. IEEE Trans Control Syst Technol. 23(1):80–90.